Iranian Journal of Analytical Chemistry
Volume 12, Issue 2, September 2025 (60-71) Original Research Article
مجله ایرانی شیمی تجزیه
دوره ۱۲، شماره ۲، مهر ۱۴۰۴ (۷۱-۶۰)

Photodegradation of hazardous anionic and cationic azo dyes using $AlCoFe_2O_4$ as a green catalyst

Rahil Sayadipour*, Homa Shafieekhani

M.Sc. Student in Analytical Chemistry, Payame Noor University, Shiraz, Iran.
Ph.D. in Analytical Chemistry, Assistant Professor, Payame Noor University, Tehran, Iran

Received: 26 July 2025 **Accepted:** 19 September 2025
DOI: 10.30473/ijac.2026.76089.1329

Abstract
Wastewater from the textile industry is classified as the most polluting of all the industrial sectors. Among these, azo dyes are one of the most important pollutants which have many toxic effects, especially carcinogenicity and mutagenicity. Thus, it is necessary to develop a powerful, eco-friendly and effective photodegradation process for the removal of azo dyes. In this study, aluminum-doped cobalt ferrite ($AlCoFe_2O_4$) nanoparticles were synthesized via co-precipitation as a green photocatalyst for the degradation of anionic and cationic azo dyes. The nanoparticles were characterized using XRD, EDS, DRS, FESEM, and VSM. The results of XRD showed that the nanoparticles had a cubic structure with an average diameter size less than 45 nm. The low remanent magnetization and coercivity of the nanoparticles in VSM was consistent with soft magnetic properties. Moreover, the magnetic properties of $AlCoFe_2O_4$ nanoparticles enable easy separation of the photocatalyst from the reaction medium using an external magnetic field. In addition, high absorption of $AlCoFe_2O_4$ in the visible light region makes it possible to increase photocatalytic performance of the photocatalyst under the influence of visible light. Photocatalytic tests using Methyl Orange (MO) and Bismarck Brown (BB) dyes showed that degradation strongly depends on pH (optimal pH ≈ 3 and 9 for MO and BB respectively), adsorption of dye molecules on the catalyst surface, and catalyst dosage (0.05 g) .Under optimized conditions, MO degradation reached 100% under UV irradiation, while BB degradation reached 98%. The photocatalyst maintained high performance over at least five cycles, demonstrating stability and recyclability.

Keywords
Green photocatalyst; Photodegradation; Azo dyes; Magnetic nanoparticles.

1. Introduction

One of the most important environmental pollutants is dye contaminants from the textile and dyeing industry that are toxic to humans and the environment [1-4]. In addition, other industries such as cosmetics, leather, pharmaceuticals, and paper factories also produce dye contaminants. Most of these dyes are very carcinogenic, even in small amounts.

Some of these pollutants may be biologically treated in the natural environment, but many of them are toxic and not biologically treatable [5-8]. Thus, these substances can remain in the environment for a long time and have harmful effects on human health and ecosystems.

Almost half of textile dye products are azo compounds whose molecular structure has a chromophore group (-N=N-). About 15-20% of the total dye produced during dyeing in the textile industry is lost and released as effluent [9]. However, azo dyes are stable with low degradability and are often soluble in water, so it is difficult to remove them from aqueous solutions by conventional purification methods.

Therefore, it is necessary to develop effective, safe, and eco-friendly methods to treat these organic pollutants. In recent years, many techniques have been studied to remove these organic pollutants from drinking water and wastewater. There are different approaches to removing these organic contaminants from aqueous solutions, including chemical, physical, electrochemical, biological, and membrane processes [10-13]. Also, some methods such as adsorption [14-17], biological treatment [18-21] and chemical oxidation [22-24], have been proposed.

However, adsorption only transfers dye pollutants from the aqueous phase to the solid phase

* Corresponding author:

R. Sayadipour; E-mail: sayadipourr@gmail.com

rather than destroying them; therefore, it cannot be considered a complete treatment method. On the other hand, biodegradation methods are useful for the complete destruction of a wide variety of contaminants. However, these methods are limited to those compounds that are biodegradable. Therefore, these processes are not very efficient for removing all pollutants.

Nowadays, finding a suitable method to solve these problems seems important and necessary. Recently, much research has been done to find easy and eco-friendly treatment methods for degradation of dye contaminants. Among these, photocatalytic oxidation using a semiconductor is an effective technique to remove these contaminants. Organic pollutants can be converted to carbon dioxide (CO_2), water (H_2O), and other simple materials in this process [25-29].

Nowadays, magnetic nanoparticles are considered by researchers due to their application in various fields such as magnetic fluids, catalysis, biotechnology, medicine, magnetic resonance imaging, information storage and environmental treatment [30-33]. Magnetic nanoparticles generally contain magnetic elements such as iron, cobalt, nickel and their chemical compounds. In recent years, magnetic nanoparticles such as spinel ferrites with the chemical composition MFe_2O_4 have been extensively studied due to the special properties they have shown. Among these, cobalt ferrite is of special importance due to the high coercivity at room temperature, balanced magnetic saturation, as well as good chemical and physical stability.

Meanwhile, some researchers have reported doped spinel ferrites with various metals in order to improve their degradation efficiency [34-36].

In the present study, the novel catalyst aluminum-doped cobalt ferrite prepared by co-precipitation method has been used to degrade cationic and anionic azo dyes. Methyl Orange (MO) and Bismarck Brown (BB) were selected as a model of anionic and cationic dyes to study the UV/Vis–H_2O_2 degradation of synthetic dyes under in the presence of the photocatalyst.

2. Experimental

2.1. Material and methods

All chemicals were of analytical grade and purchased from Sigma-Aldrich. Deionized water served as reacting medium. Adjustment of pH was performed by 0.01 M HCl and/or 0.01 M NaOH solutions. The UV irradiation source consisted of two 30 W mercury lamps placed above a batch photoreactor. XRD patterns were recorded using powder X-ray diffraction (Bruker make diffractometer, Cu-Kα X-rays of wavelength λ=1.5406 Å). SEM images were obtained using a scanning electron microscope (FE-SEM, Mira3 Tescan).

Table 1. List of chemicals and reagents used in this study.

Material Name	Chemical Formula	Amount (g or ml)	Application
Cobalt(II) nitrate	$Co(NO_3)_2{\cdot}6H_2O$	2 g	Cobalt source for $AlCoFe_2O_4$ synthesis
Iron(III) chloride	$FeCl_3{\cdot}6H_2O$	4.33 g	Iron source for $AlCoFe_2O_4$ synthesis
Aluminum sulfate	$Al_2(SO_4)_3{\cdot}6H_2O$	1.99 g	Aluminum source for $AlCoFe_2O_4$ synthesis
Polyethylene glycol (PEG)	Polymer	1 g	Surfactant for size/morphology control
Ammonia (25%)	NH_3 (aq)	As required for pH adjustment	pH adjustment in co-precipitation
Deionized water	H_2O	100 ml	Solvent and washing agent
Methyl Orange (MO)	$C_{14}H_{14}N_3NaO_3S$	30 ppm (50 ml)	Anionic azo dye for photodegradation
Bismarck Brown (BB)	$C_{21}H_{24}N_6{\cdot}2HCl$	30 ppm (50 ml)	Cationic azo dye for photodegradation
Hydrochloric acid	HCl (0.01 M)	As required for pH adjustment	pH adjustment of dye solutions
Sodium hydroxide	NaOH (0.01 M)	As required for pH adjustment	pH adjustment of dye solutions
Hydrogen peroxide	H_2O_2	0.5 ml	Oxidizing agent for photocatalysis

DOI: 10.30473/ijac.2026.76089.1329

2.2. Synthesis of photocatalyst

$AlCoFe_2O_4$ was synthesized by co-precipitation method by using analytical grade constituent metal salts. $Co(NO_3)_2.6H_2O$ (2 g) and $FeCl_3.6H_2O$ (4.33 g) and $Al_2(SO_4)_3.6H_2O$ (1.99 g) were dissolved in 100 mL of deionized water. Polyethylene glycol (1 gr) as surfactant was added in this step. PEG is a water-soluble polymer and is generally considered a non-toxic and biodegradable polymer, minimizing the environmental impact compared to many organic solvents traditionally employed in nanoparticle synthesis. The mixture was stirred continuously at room temperature for 30 min and then ammonia solution (25%) was added to reach pH = 8, and stirring was continued for 1 h at 60 °C. Finally, the obtained precipitate was washed several times with deionized water, filtered and dried at 70 °C.

The resulting powder was then calcined at 450 °C for 3 h. Calcination is a necessary step for achieving the desired crystalline structure; the overall synthesis route avoids the use of hazardous organic solvents, minimizes waste generation, and operates under relatively mild conditions. The structure of the magnetic nanoparticle was characterized by powder X-ray diffraction (XRD), scanning electron microscopy (SEM-EDS), vibrating sample magnetometry (VSM), diffuse reflectance spectroscopy and UV-Vis spectroscopy [37].

2.3. Photocatalytic activity

The photocatalytic efficiency of the synthesized magnetic nanoparticles was investigated by changing some physical parameters such as pH, different photocatalyst dosages, contact time, and different concentrations of dye on the degradation process. The UV irradiation source consisted of two 30 W mercury lamps placed above a batch photoreactor.

Methyl Orange and Bismarck Brown were used as representatives of anionic and cationic dyes to investigate photocatalytic degradation. Adjustment of pH was performed by 0.01 M HCl and/or 0.01M NaOH solutions.

A 50 ml dye solution (30 ppm) different dosages of photocatalyst were added and the mixture was stirred in the dark for 30 minutes to achieve better dispersion and adsorption performance before degradation. The pH of the dye solution was adjusted and then 0.5 ml of H_2O_2 was added to the solutions as an oxidant. Then the mixtures were exposed to visible or ultraviolet light irradiation. At degradation intervals of 30 minutes, the absorbance of the sample solutions was determined using a UV-Vis spectrophotometer at the maximum absorbance wavelength of each dye.

Degradation efficiency of the photocatalytic processes was evaluated by the degradation ratio (D), as follows:

$$\%D = \left[\frac{C_0 - C}{C_0}\right] \times 100 \qquad (1)$$

Where C_0 and C_t were the initial and the time-dependent concentrations, respectively and D% denotes the degradation rate.

3. Result and Discussion

3.1. Characterization of the nanocatalyst

XRD patterns of $AlCoFe_2O_4$ (Fig. 1) were recorded using powder X-ray diffraction (Bruker make diffractometer, Cu-Kα X-rays of wavelength λ = 1.5406 Å). The single phase formation of pure nanoparticles was confirmed by the sharp peaks at 2θ (23.74, 29.89, 35.52, 43.14, 54.16, 57.10, 62.99), which are accredited to (111), (220), (311), (400), (422), (511) and (440). All the peaks were indexed within a single phase cubic spinel structure with Fd3m space group (JCPDS Card No. 86-2267).

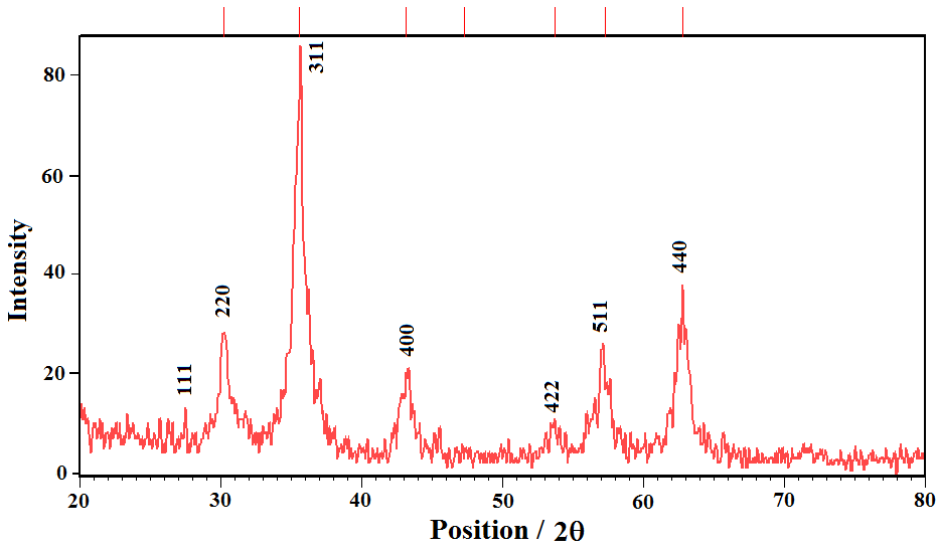

Fig. 1. XRD patterns of $AlCoFe_2O_4$

DOI: 10.30473/ijac.2026.76089.1329

The crystallite size was calculated from intensity of the highly diffracted peak (311) according to the Debye-Scherrer formula giving the crystal size of 6.63 nm. Quantitative analysis of synthesized nanocatalyst was performed using EDS (Figure 2). The obtained results proved the presence of Al, Co, Fe, and O with 7.46, 9.73, 24.70 and 58.12 atomic percentage respectively.

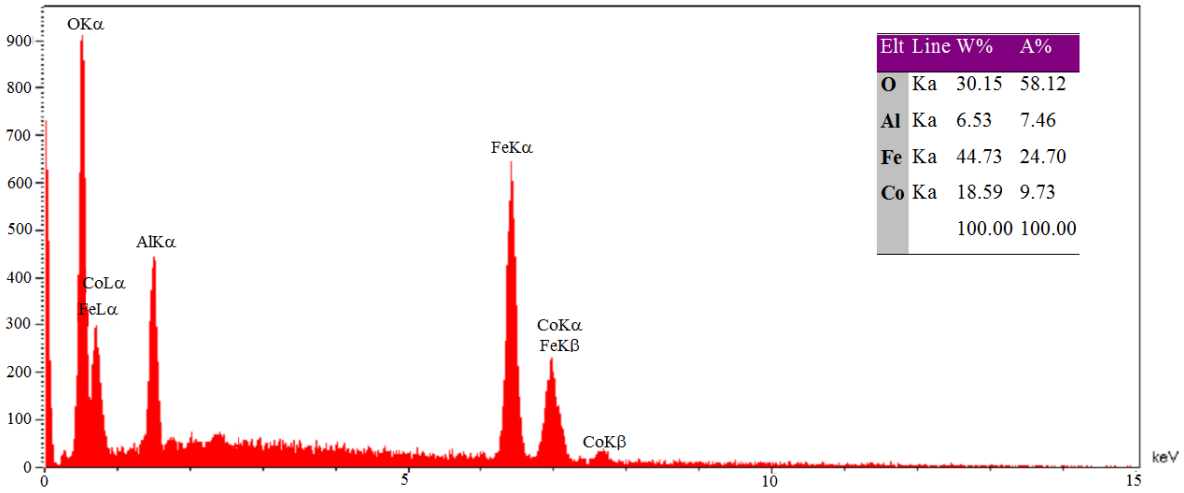

Fig. 2. EDS image of $AlCoFe_2O_4$

The above results confirmed that the prepared material was $AlCoFe_2O_4$, without any impurities.

Figure 3 illustrates the SEM image of synthesized $AlCoFe_2O_4$ nanocrystals (FE-SEM, Mira3 Tescan). As can be seen in this micrograph, the nanoparticles were cubicshaped with an average diameter less than 45 nm with some agglomeration. The cubic structure of spinel ferrites is primarily attributed to the distribution of Co^{2+} ions in the octahedral sites, which effectively suppresses cooperative Jahn–Teller distortion.

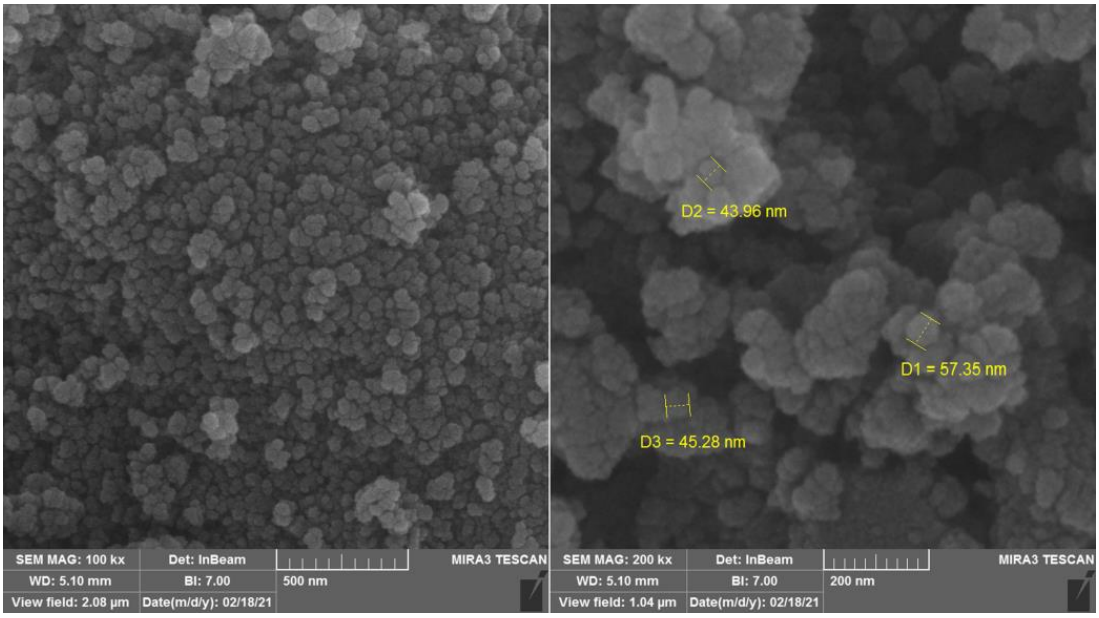

Fig. 3. FESEM image of $AlCoFe_2O_4$ nanocrystals

Couplings at the atomic level, including the coupling between electron spins and between the electron spin and the angular momentum of the electron orbital are two factors that create magnetic properties of materials.

DOI: 10.30473/ijac.2026.76089.1329

Figure 4 shows the hysteresis loops of $AlCoFe_2O_4$ nanoparticles measured using a vibrating sample magnetometer (VSM).

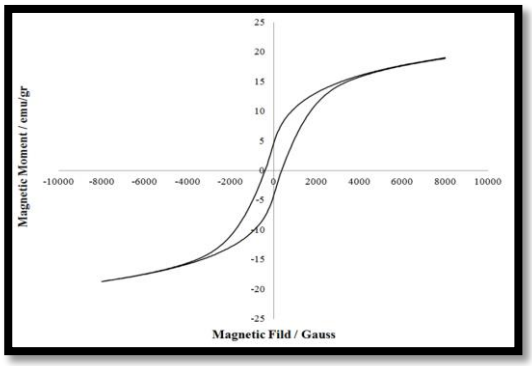

Fig. 4. Vibrating sample magnetometer of $AlCoFe_2O_4$ nanoparticles

As can be seen, the saturation magnetization (M_s), remanent magnetization (M_r), and coercivity (H_c) values obtained for the sample were 18.05 emu/g, 4.44 emu/g, and 394 Oe, respectively. The low remanent magnetization and coercivity of the nanoparticles are consistent with the properties of the soft magnetic materials.

Diffuse reflectance (DRS) spectra of the sample were recorded using a V-670, JASCO spectrophotometer (Figure 5).

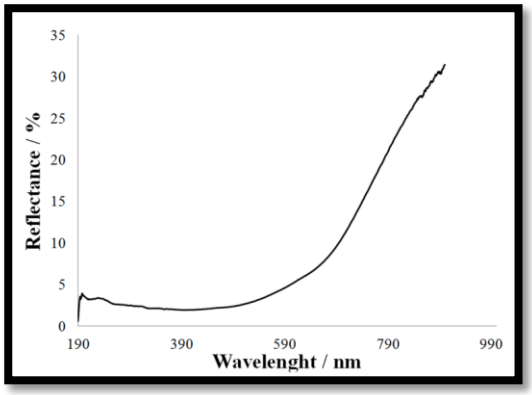

Fig. 5. DRS spectra of $AlCoFe_2O_4$

UV–Vis spectra of $AlCoFe_2O_4$ was compared with $CoFe_2O_4$ nanocatalyst in figure 6.

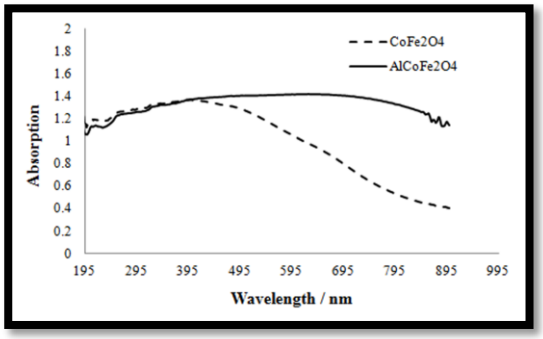

Fig. 6. UV–Vis spectra of $AlCoFe_2O_4$ and $CoFe_2O_4$As can be seen, higher absorption of $AlCoFe_2O_4$ in the visible light region makes it possible to increase the photocatalytic performance of the photocatalyst under visible light irradiation.

3.2. Photocatalytic activity

The operation of semiconductor compounds in photocatalytic reactions can be summarized as follows. First, the absorption of photons by the semiconductor compound creates electron-hole pairs, which then propagate to the surface of the semiconductor and react with the adsorbed pollutant particles at the active sites on the surface. In this reaction, e^- and h^+ act as strong reducing and oxidizing agents, respectively. Finally, the decomposition of pollutants is driven by charge carriers. Adding small amounts of H_2O_2 as an auxiliary oxidizer improves the performance of the photocatalyst.

Therefore, the degradation efficiency of the synthesized photocatalyst strongly depends on the adsorption of dye molecules on the catalyst surface. On the other hand, the pH of the solution can affect the amount of dye adsorption.

Therefore, to determine the optimal conditions for dye adsorption on the surface of the catalyst, the point of zero charge of the catalyst was determined using the drift method [38]. As the results show, the pH_{PZC} value of the synthesized $AlCoFe_2O_4$ was 5.8. It means that at this pH, the net surface charge on catalyst is zero. However, the surface of photocatalyst has a net positive charge at $pH < pH_{PZC}$, while it has a net negative charge at $pH > pH_{PZC}$.

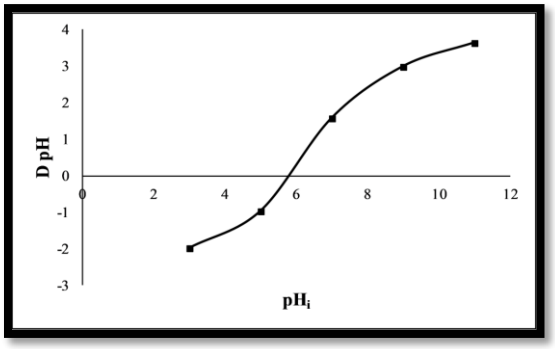

Fig. 7. Point of zero charge of $AlCoFe_2O_4$ nanocatalyst

Therefore, it is expected that the electrostatic attraction between the MO (negative ions) and the positively charged of the photocatalyst surface is observed at pH < 6.35. In contrast, electrostatic attraction between the BB cations (positive ions) and the negatively charged surface of photocatalyst is observed at pH > 6.35. In order to determine the optimal pH in the degradation process, the experiments were performed in the range pH = 3, 4, 5, and pH = 7, 8, 9 for MO and BB respectively. The degradation after 60 minutes is shown in table 1.

DOI: 10.30473/ijac.2026.76089.1329

As can be seen in Table 3, adsorption of both dyes was low at pH = 6 and reached a maximum value in the pH = 3 and 9 for MO and BB respectively.

Table 2. Optimization of initial pH.

dye	pH=3	pH=4	pH=5	pH=7	pH=8	pH=9
MO	100	54.47	29.73	-	-	-
BB	-	-	-	30.56	44.21	82.84

To evaluate the photocatalyst dosage, degradation of MO was selected as the model reaction. Degradation process was performed using different amounts of photocatalyst. As can be seen in Figure 8, the degradation of MO is enhanced with increasing the dosage of photocatalyst. Considering the removal efficiency and reagent cost, 0.05 g of photocatalyst was chosen for the degradation process in the following tests.

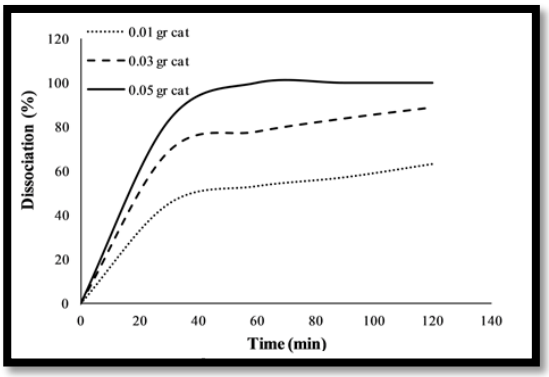

Fig. 8. Influence of photocatalyst dosage on the degradation.

According to the results obtained, HCl and NaOH were used to adjust the initial solution pH to the desired value for each dye. At first, adsorption of MO and MB on the photocatalyst surface was performed in the dark for 30 minutes to achieve adsorption equilibrium. Then the mixtures were exposed to visible or ultraviolet light irradiation. At degradation intervals of 30 minutes, the absorbance of the sample solutions was determined using a UV spectrophotometer at the maximum absorbance wavelength of each dye. The results are summarized in Figures 9 and 10.

Figure 9 shows degradation efficiency under UV irradiation. As can be seen, the photodegradation of Methyl Orange increased rapidly and reached 100% after 60 minutes. However, the optical degradation of BB increased gradually, reaching 98% after 180 minutes.

Experiments performed under visible light showed that the photocatalytic performance increased over time and reached 62.37% and 97.6% degradation after three hours for BB and MO, respectively. This shows that the $AlCoFe_2O_4$ photocatalyst can be used effectively under visible light for photocatalytic applications. As can be seen, the catalytic activity of $AlCoFe_2O_4$ nanoparticles in the photodegradation of MO was significantly higher than that of BB in both UV and visible light irradiation.

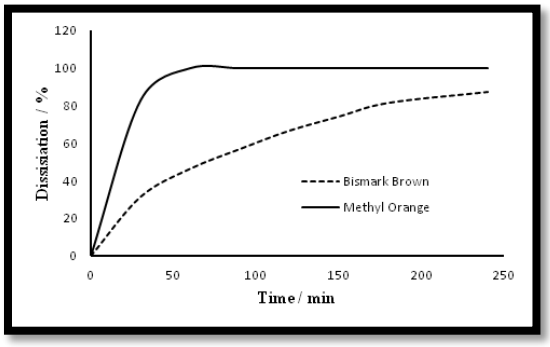

Fig. 9. Dissociation curve of MO and BB under UV irradiation.

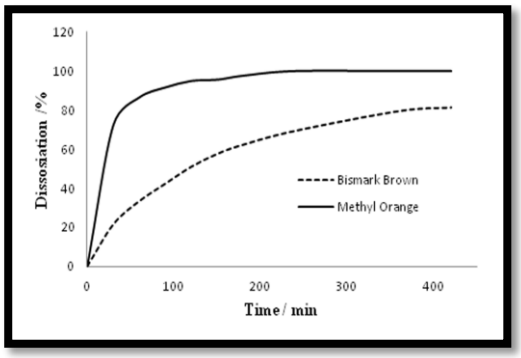

Fig. 10. Dissociation curve of MO and BB under Vis irradiation.

As shown in Figures 11 and 12, the data were well fitted to a pseudo-first-order equation. The plot of $\ln(C_0/C)$ versus t provides a linear relationship, and the reaction rates (k values) are determined from the slope of the plot. Reaction rates were equal to 8.00×10^{-2} min^{-1} (MO) and 8.50×10^{-3} min^{-1} (BB).

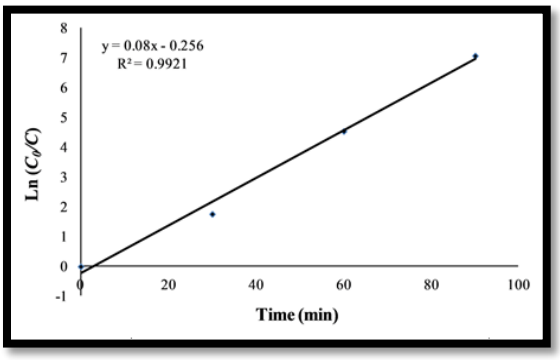

Fig. 11. Kinetics of MO removal.

DOI: 10.30473/ijac.2026.76089.1329

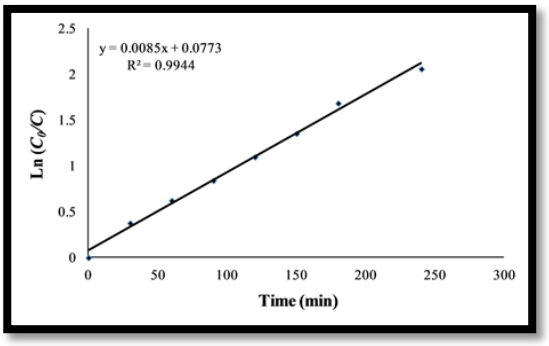

Fig. 12. Kinetics of BB removal.

The stability and the reusability of the nanocatalyst were also investigated. The photocatalytic efficiency of the nanocatalyst was evaluated for five cycles by catalyst recovery only by washing with water and acetone and drying at 100° C. The results showed that the recycled photocatalyst maintained good performance after five cycles.

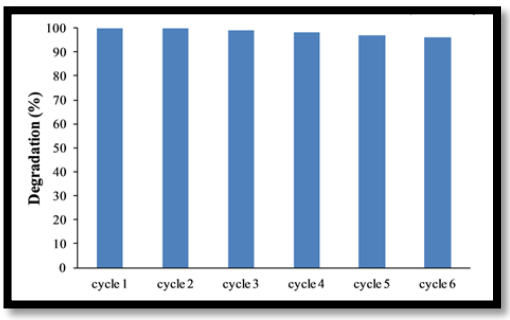

Fig. 13. Reusability of photocatalyst.

However, the recycled photocatalyst showed a 4% reduction in performance after six uses.

The results showed that $AlCoFe_2O_4$ has the potential to be used for cost-effective treatment of dye-contaminated wastewater under visible irradiation.

3.3. Mechanism of photocatalytic degradation of MO and BB

The efficient degradation of azo dyes such as Methyl Orange (MO) and Bismarck Brown (BB) mediated by $AlCoFe_2O_4$ nanoparticles under UV/Vis irradiation in the presence of hydrogen peroxide is attributed to a synergistic effect between adsorption, photo-generated charge carriers, and activated oxygen species. The proposed mechanism, drawing upon the observed performance and established pathways in similar semiconductor photocatalytic systems, is delineated below.

3.3.1. Light absorption and electron–hole pair generation

The $AlCoFe_2O_4$ spinel ferrite, exhibiting significant absorption in the UV and visible regions of the spectrum (cf. Figures 5 and 6), readily absorbs incident photons. Photons with energy greater than or equal to the catalyst's band gap energy induce the excitation of electrons from the valence band (VB) to the conduction band (CB), consequently generating holes (h^+) in the VB:

$$AlCoFe_2O_4 + h\nu \rightarrow e^-_{CB} + h^+_{VB}$$

3.3.2. Generation of reactive oxygen species (ROS)

The photogenerated charge carriers, alongside the added H_2O_2, are crucial for initiating the oxidative degradation process. The interaction of H_2O_2 with the photocatalyst system typically leads to the formation of highly reactive species, primarily hydroxyl radicals (•OH):

- Reaction with conduction band electrons: Electrons in the CB can react with H_2O_2 to produce hydroxyl radicals:

$$H_2O_2 + e^-_{CB} \rightarrow \bullet OH + OH^-$$

Direct photolysis of H_2O_2: Under UV/Vis irradiation, H_2O_2 can also undergo direct decomposition to yield hydroxyl radicals:

$$H_2O_2 + h\nu \rightarrow 2 \bullet OH$$

Catalyst-mediated activation: The inherent properties of the $AlCoFe_2O_4$ catalyst, particularly the presence of transition metal ions like Fe and Co, can facilitate the decomposition of H_2O_2 through Fenton-like or photo-Fenton processes, further enhancing •OH generation.

Simultaneously, photogenerated holes in the VB can also contribute to the generation of •OH radicals through reactions with adsorbed water molecules or hydroxide ions:

$$h^+_{VB} + H_2O \rightarrow \bullet OH + H^+$$

$$h^+_{VB} + OH^- \rightarrow \bullet OH$$

3.3.3. Surface adsorption and dye oxidation

The observed high degradation efficiencies, particularly in conjunction with the reported pH-dependent adsorption characteristics (pH_{pzc} = 5.8; optimal MO degradation at pH = 3, BB at pH= 9), underscore the critical role of surface adsorption. Dye molecules are initially adsorbed onto the catalyst surface, concentrating them in proximity to the active sites where ROS are generated.

The adsorbed dye molecules are then subjected to oxidative attack by the photogenerated holes and, more significantly, the hydroxyl radicals. This direct or indirect oxidation breaks down the complex organic structure of the azo dyes:

$$Dye_{adsorbed} + \bullet OH \rightarrow Oxidation\ Intermediates$$

DOI: 10.30473/ijac.2026.76089.1329

$$Dye_{adsorbed} + h^{+}_{VB} \rightarrow Oxidation\ Products$$

3.3.4. Mineralization

Through a series of intermediate oxidation steps, the organic dyes are ultimately mineralized into simpler, inorganic compounds such as carbon dioxide, water, and various inorganic ions.

Oxidation Intermediates → $CO_2 + H_2O$ + Inorganic Ions

This mineralization pathway is a hallmark of effective advanced oxidation processes.

3.4. Comparative evaluation of the proposed photocatalyst with previously reported systems

A comparative analysis of the present $AlCoFe_2O_4$ photocatalytic system against benchmark technologies reveals distinct mechanistic and operational advantages (Table. 2 and Table. 3). As documented by Hosseini et al. (2025), the Co_3O_4/g-C_3N_4 nanonet composite utilizes an S-scheme heterojunction architecture to achieve 97% sertraline degradation within 60 min, relying on the synergistic production of •OH and $•O_2^-$ radicals [39]. This AOP approach is fundamentally distinct from the $NaBH_4$-mediated catalytic reduction systems extensively reviewed by Naz et al. (2021). While the latter systems demonstrate exceptional kinetics, often achieving >98% dye reduction in under 5 minutes (e.g., Pd/walnut shell at 0.21 min and AgNPs/clinoptilolite at 138 s; [40]), they are thermodynamically constrained by the continuous consumption of chemical reductants and function primarily as electron relays (redox mediators). Furthermore, many high-performance reduction catalysts rely on noble metals such as Pd, Au, or Ag (Tables 4–6, [40]), which increase synthesis costs and industrial scalability challenges. In contrast, the $AlCoFe_2O_4$ spinel system proposed herein achieves highly efficient oxidative degradation—leading to mineralized products like CO_2 and H_2O—without the requirement for noble metal dopants or external chemical reductants. By leveraging intrinsic magnetic properties for rapid catalyst recovery and maintaining stability over multiple cycles, the $AlCoFe_2O_4$ system offers a more sustainable and economically viable pathway for large-scale wastewater decontamination, effectively balancing reaction kinetics with the environmental imperative of complete pollutant mineralization.

Table 3. Comparative evaluation of the proposed photocatalyst with previously reported systems.

Study / Reference	Catalyst dosage	Reaction time	Degradation / Removal efficiency	Kinetic model	Reactive species / Mechanism	Key advantages
Present study ($AlCoFe_2O_4$ photocatalyst)	0.05 g / 50 ml	60 min (MO)	100% MO degradation under UV; 98% BB degradation	Pseudo-first-order	Hydroxyl radicals (•OH), photogenerated holes (h^+)	Magnetic separation, green synthesis, stable up to 5 cycles
Hosseini (2025) – Environmental Science and Pollution Research [39]	10 mg / 100 ml	60 min	~97% degradation efficiency	First-order ($k = 0.0536\ min^{-1}$)	S-scheme heterojunction mechanism generating •OH and $•O^{2-}$ radicals	High surface area porous nanonet structure and improved charge separation
Chitosan adsorption study [42]	0.1 g CS solution	1 min	99.9% CR removal; adsorption capacity up to 44956 mg. g^{-1}	Adsorption equilibrium	Electrostatic adsorption between dye molecules and CS	Ultra-fast removal and extremely high adsorption capacity
Naz et al. (2021) – Journal of Materials Science (Review) [40]	Depends on catalyst	Usually minutes	High degradation efficiencies reported	Pseudo-first-order in many systems	Electron transfer via redox mediator between $NaBH_4$ and dye molecules	Simple operation and rapid degradation
Panahimehr et al. (Pd/$ZnMn_2O_4$/Chitosan) [41]	20 mg	12 min	Very high degradation efficiency	Pseudo-first-order ($R^2 = 0.9948$)	Reactive oxygen species including $•O^{2-}$ and •OH radicals	SPR effect of Pd nanoparticles, visible light activity and recyclability up to 7 cycles

DOI: 10.30473/ijac.2026.76089.1329

Table 3. Comparative evaluation of the proposed photocatalyst with previously reported systems.

Study / Reference	Pollutant type	Treatment process	Catalyst / Material	Light source	Initial concentration
Present study ($AlCoFe_2O_4$ photocatalyst)	Azo dyes: Methyl Orange (MO), Bismarck Brown (BB)	Photocatalytic degradation (AOP) with H_2O_2	Magnetic spinel ferrite $AlCoFe_2O_4$ nanoparticles	UV (30 W mercury lamps) and visible light	30 $mg.L^{-1}$
Hosseini (2025) – Environmental Science and Pollution Research [39]	Sertraline (pharmaceutical pollutant)	Visible-light photocatalysis	Co_3O_4/g-C_3N_4 nanonet structured composite	Xenon lamp 300 W (350–780 nm visible light)	75 $mg.L^{-1}$
Chitosan adsorption study [42]	Congo Red (CR), Methylene Blue (MB), Rhodamine B (RhB)	Adsorption	Chitosan (CS) and CS-CR particles	No light required	500–2000 $mg.L^{-1}$
Naz et al. (2021) – Journal of Materials Science (Review) [40]	Organic dyes (MO, MB, CR, nitrophenols)	Catalytic chemical reduction	Various metal and bimetallic nanoparticles with $NaBH_4$	No light required	Variable
Panahimehr et al. ($Pd/ZnMn_2O_4$/Chitosan) [41]	Congo Red dye	Sunlight-assisted photocatalytic degradation	$Pd/ZnMn_2O_4$/chitosan nanobiocatalyst	Natural sunlight	5 $mg.L^{-1}$

Conclusion

In this research, $AlCoFe_2O_4$ nanoparticles were successfully synthesized through a simple and efficient co-precipitation route and demonstrated multifunctional characteristics suitable for photocatalytic wastewater treatment. Structural and morphological studies confirmed the formation of uniform cubic nanoparticles with an average size below 45 nm. The magnetic analysis revealed soft magnetic behavior with low remanence and coercivity, enabling facile magnetic separation and reusability—advantages crucial for sustainable applications.

The surface charge properties, characterized by a pH_{pzc} of 5.8, strongly influenced the adsorption of dyes. Maximum adsorption of Methyl Orange (MO) and Bismarck Brown (BB) occurred at pH = 3 and pH = 9, respectively, underscoring the decisive role of surface–dye interaction in determining overall photocatalytic efficiency. This dependence highlighted adsorption as a key step preceding the photo-oxidation process.

Under UV/Vis irradiation in the presence of H_2O_2, the $AlCoFe_2O_4$ nanocatalyst exhibited remarkable photocatalytic performance, achieving complete degradation of MO (100%) and high degradation of BB (98% under UV and 62.37% under visible light). The observed activity reflects the synergistic effect of its efficient light absorption, effective charge separation, strong adsorption ability, and generation of reactive oxygen species (•OH and h^+), as discussed in the proposed mechanism.

Overall, the obtained results confirm that $AlCoFe_2O_4$ is a promising, magnetically separable, and cost-effective photocatalyst capable of operating under both UV and visible illumination. Its combination of high activity, structural stability, and recyclability positions it as a viable material for the treatment of dye-contaminated wastewater and other organic pollutants, contributing to environmentally benign water purification technologies.

Acknowledgments

The authors wish to acknowledge the support of this work by Payame Noor University Research council.

References

[1] N.R. Vaghela and K. Nath. Modelling and multi-objective optimization of continuous indirect electro-oxidation process for RTB21 dye wastewater using ANN-GA approach. Acta Chim. Slov. 69 (2022) 304-315.

[2] S. Findik. Removal of diazo dye Direct Red 28 and tetra azo dye Direct Black 22 using synthesized magnetic kaolin supported zinc ferrite. Acta Chim. Slov. 69 (2022) 336-348. http://dx.doi.org/10.17344/acsi.2021.7289

[3] U. Jayaram and M.A. Azam. Computational molecular modeling studies of some Mycobacterium tuberculosis alanine racemase inhibitors. Acta Chim. Slov. 69 (2022) 393-404. http://dx.doi.org/10.17344/acsi.2021.7267

[4] N.S. Gilani, S.E. Tilami and S.N. Azizi. Adsorption properties of low-cost synthesized nanozeolite L for efficient removal of toxic methylene blue dye from aqueous solution. Acta Chim. Slov. 69 (2022) 458-465. http://dx.doi.org/10.17344/acsi.2022.7350

[5] N.Y. Donkadokula, A.K. Kola, I. Naz and D. Saroj. A review on advanced physico-chemical and biological textile dye wastewater treatment

techniques. Rev. Environ. Sci. Biotechnol. 19 (2020) 543-560. https://doi.org/10.1007/s11157-020-09543-z
[6] A. Alhujaily, H. Yu, X. Zhang and F. Ma. Adsorptive removal of anionic dyes from aqueous solutions using spent mushroom waste. Appl. Water Sci. 10 (2020) 1-12. https://doi.org/10.1007/s13201-020-01268-2
[7] A. Ahmadi, R. Foroutan, H. Esmaeili and S. Tamjidi. The role of bentonite clay and bentonite clay@MnFe2O4 composite and their physico-chemical properties on the removal of Cr (III) and Cr (VI) from aqueous media. Environ. Sci. Pollut. Res. 27 (2020) 14044-14057. https://doi.org/10.1007/s11356-020-07756-x
[8] D.A. Yaseen and M. Scholz. Textile dye wastewater characteristics and constituents of synthetic effluents: a critical review. Int. J. Environ. Sci. Technol. 16 (2019) 1193-1226. https://doi.org/10.1007/s13762-018-2130-z
[9] S. Temel, E. Yaman, N. Ozbay and F.O. Gokmen. Synthesis, characterization and adsorption studies of nano-composite hydrogels and the effect of SiO_2 on the capacity for the removal of methylene blue dye. J. Serb. Chem. Soc. 85 (2020) 939-952. https://doi.org/10.2298/JSC190517114T
[10] M.D. Khan, A. Singh, M.Z. Khan, S. Tabraiz and J. Sheikh. Current perspectives, recent advancements, and efficiencies of various dye-containing wastewater treatment technologies. J. Water Process Eng. 53 (2023) 103579. https://doi.org/10.1016/j.jwpe.2023.103579
[11] L.D. Paquini, L.T. Marconsini, L.P.R. Profeti, O.S. Campos, D. Profeti and J. Ribeiro. An overview of electrochemical advanced oxidation processes applied for the removal of azo dyes. Braz. J. Chem. Eng. 40 (2023) 623-653. https://doi.org/10.1007/s43153-023-00300-7
[12] H. Solayman, M.A. Hossen, A. Abd Aziz, N.Y. Yahya, K.H. Leong, L.C. Sim, M.U. Monir and K.-D. Zoh. Performance evaluation of dye wastewater treatment technologies: a review. J. Environ. Chem. Eng. 11 (2023) 109610. https://doi.org/10.1016/j.jece.2023.109610
[13] I.A. Shah, M. Bilal, I.W. Almanassra and I. Ihsanullah. A comprehensive review of graphene oxide-based membranes for efficient dye removal from water sources. Sep. Purif. Technol. 330 (2024) 125277. https://doi.org/10.1016/j.seppur.2023.125277
[14] T.Y. Ying, A.A.A. Raman, M.M. Bello and A. Buthiyappan. Magnetic graphene oxide-biomass activated carbon composite for dye removal. Korean J. Chem. Eng. 37 (2020) 2179-2191. https://doi.org/10.1007/s11814-020-0628-9
[15] B. Zhou, Y. Tang, L. Zhao, L. Guo and J. Zhou. Novel Fe3O4–poly (methacryloxyethyltrimethyl ammonium chloride) adsorbent for the ultrafast and efficient removal of anionic dyes. RSC Adv. 11 (2021) 1172-1181. https://doi.org/10.1039/D0RA09296G
[16] Z. Duan, Y. Li, M. Zhang, H. Bian, Y. Wang, L. Zhu and D. Xia. Towards cleaner wastewater treatment for special removal of cationic organic dye pollutants: a case study on application of supramolecular inclusion technology with β-cyclodextrin derivatives. J. Clean. Prod. 256 (2020) 120308. https://doi.org/10.1016/j.jclepro.2020.120308
[17] T. Li, H.L. Song, H. Xu, X.L. Yang and Q.L. Chen. Biological detoxification and decolorization enhancement of azo dye by introducing natural electron mediators in MFCs. J. Hazard. Mater. 416 (2021) 125864. https://doi.org/10.1016/j.jhazmat.2021.125864
[18] E. Danso-Boateng, E. Nyktari, A.D. Wheatley, R.G. Holdich and A.S. Mohammed. Production and characterisation of adsorbents synthesised by hydrothermal carbonisation of biomass wastes. Water Air Soil Pollut. 231 (2020) 1. https://doi.org/10.1007/s42452-021-04273-5
[19] C. Ram, P. Rani, K.A. Gebru and M.G.M. Abrha. Pulp and paper industry wastewater treatment: use of microbes and their enzymes. Phys. Sci. Rev. 5 (2020) 20190050. https://doi.org/10.1515/psr-2019-0050
[20] E. Routoula and S.V. Patwardhan. Degradation of anthraquinone dyes from effluents: a review focusing on enzymatic dye degradation with industrial potential. Environ. Sci. Technol. 54 (2020) 647-664. https://doi.org/10.1021/acs.est.9b03737
[21] K.O. Badmus, J.O. Tijani, E. Massima and L. Petrik. Treatment of persistent organic pollutants in wastewater using hydrodynamic cavitation in synergy with advanced oxidation process. Environ. Sci. Pollut. Res. 25 (2018) 7299-7314. https://doi.org/10.1007/s11356-017-1171-z
[22] H. Fattahimoghaddam, T. Mahvelati-Shamsabadi and B.K. Lee. Efficient photodegradation of rhodamine B and tetracycline over robust and green g-C3N4 nanostructures: supramolecular design. J. Hazard. Mater. 403 (2020) 123703. https://doi.org/10.1016/j.jhazmat.2020.123703
[23] J.E. Kumar, T. Mulai, W. Kharmawphlang, R.N. Sharan and M.K. Sahoo. Experimental studies on the removal of aluminium ions from synthetic aqueous solution by hydroxyapatites. Acta Chim. Slov. 68 (2021) 833-848. http://dx.doi.org/10.17344/acsi.2021.6830
[24] S.P. Goutam, G. Saxena, V. Singh, A.K. Yadav, R.N. Bharagava and K.B. Thapa. Green synthesis of TiO_2 nanoparticles using leaf extract of Jatropha curcas L. for photocatalytic degradation of tannery wastewater. Chem. Eng. J. 336 (2018) 386-396. https://doi.org/10.1016/j.cej.2017.12.029
[25] A. Khalil, N.M. Aboamera, W.S. Nasser, W.H. Mahmoud and G.G. Mohamed. Photodegradation of organic dyes by PAN/SiO_2-TiO_2-NH_2 nanofiber membrane under visible light. Sep. Purif. Technol. 224

(2019) 509-514. https://doi.org/10.1016/j.seppur.2019.05.056
[26] Q.U. Ain, U. Rasheed, M. Yaseen, H. Zhang and Z. Tong. Superior dye degradation and adsorption capability of polydopamine modified Fe_3O_4-pillared bentonite composite. J. Hazard. Mater. 397 (2020) 122758. https://doi.org/10.1016/j.jhazmat.2020.122758
[27] A. Kumar, S.K. Sharma and G. Sharma. Wide spectral degradation of norfloxacin by Ag@$BiPO_4$/BiOBr/$BiFeO_3$ nano-assembly: elucidating the photocatalytic mechanism under different light sources. J. Hazard. Mater. 364 (2019) 429-440. https://doi.org/10.1016/j.jhazmat.2018.10.060
[28] P. Mehdizadeh, Y. Orooji, O. Amiri, M. Salavati-Niasari and H. Moayedi. Green synthesis using cherry and orange juice and characterization of $TbFeO_3$ ceramic nanostructures and their application as photocatalysts under UV light for removal of organic dyes. J. Clean. Prod. 252 (2020) 119765. https://doi.org/10.1016/j.jclepro.2019.119765
[29] A. Saljooqi, T. Shamspur and A. Mostafavi. Synthesis and photocatal
N.S. Mirbagheri and S. Sabbaghi. A natural kaolin/γ-Fe_2O_3 composite as an efficient nano-adsorbent for removal of phenol from aqueous solutions. Microporous Mesoporous Mater. 259 (2018) 134-141. https://doi.org/10.1016/j.micromeso.2017.10.007
[30] S. Tabari, A.R. Pourali and E. Nazarzadeh Zare. Magnetic nanoparticles linked to pyridinium hydrotribromide groups as catalysts for selective oxidation of alcohols and protection of alcohols. Acta Chim. Slov. 69 (2022) 271-280. http://dx.doi.org/10.17344/acsi.2021.6761
[31] B. Erdem, S. Erdem and N. Tekin. Cationic surfactant templated synthesis of magnetic mesoporous nanocomposites for efficient removal of light green. Korean J. Chem. Eng. 38 (2021) 1425-1437. https://doi.org/10.1007/s11814-021-0829-x
[32] P.M. Martins, A.C. Lima, S. Ribeiro, S.L. Mendez and P. Martins. Magnetic nanoparticles for biomedical applications: from the soul of the earth to the deep history of ourselves. ACS Appl. Bio Mater. 4 (2021) 5839-5870. https://doi.org/10.1021/acsabm.1c00440
[33] J. Heydaripour, M. Gazi, A.A. Oladipo and H.O. Gulcan. Porous magnetic resin-g-chitosan beads for adsorptive removal of phenolic compounds. Int. J. Biol. Macromol. 123 (2019) 1125-1131. https://doi.org/10.1016/j.ijbiomac.2018.11.168
[34] S. Moradi, M. Moradian and H. Naeimi. Efficient one-pot synthesis of 1,4-dihydropyridines catalyzed by magnetic $MnFe_2O_4$ nanoparticles. Acta Chim. Slov. 69 (2022) 349-358. http://dx.doi.org/10.17344/acsi.2021.7238
[35] Y. Peng, G. Ye, Y. Du, L. Zeng, J. Hao, S. Wang and J. Zhou. Fe_3O_4 hollow nanospheres on graphene oxide as an efficient heterogeneous photo-Fenton catalyst for the advanced treatment of biotreated papermaking effluent. Environ. Sci. Pollut. Res. 28 (2021) 39199-39209. https://doi.org/10.1007/s11356-021-13458-9
[36] F. Mostaghni, H. Shafiekhani and N. Madadi Mahani. A facile synthesis of bioactive five- and six-membered N-heterocyclic aromatic compounds using $AlCoFe_2O_4$ as a green catalyst. Acta Chim. Slov. 69 (2022) 91-97. https://doi.org/10.17344/acsi.2021.7021
[37]H.N. Tran, Y.F. Wang, S.J. You and H.P. Chao. Insights into the mechanism of cationic dye adsorption on activated charcoal: the importance of π–π interactions. Process Saf. Environ. Prot. 107 (2017) 168-180. https://doi.org/10.1016/j.psep.2017.02.010
[38] M. Hosseini. Visible-light-assisted decontamination of sertraline in water using a Co_3O_4/g-C_3N_4 nanocomposite photocatalyst. Environ. Sci. Pollut. Res. 32 (2025) 20441–20460. https://doi.org/10.1007/s11356-025-36848-9
[39] M. Naz. A. Rafiq. M. Ikram. A. Haider. S.O.A. Ahmad. J. Haider and S. Naz. Elimination of dyes by catalytic reduction in the absence of light: A review. J. Mater. Sci. 56 (2021). https://doi.org/10.1007/s10853-021-06279-1
[40] M. Panahimehr. S. Asghari. M. Hosseini and A. Mojaddami. Pd/ZnMn2O4/chitosan nanobiocatalyst: A sustainable solution for sunlight-enhanced photocatalytic degradation of Congo red dye. J. Mol. Struct. (2025). https://doi.org/10.1016/j.molstruc.2025.143339
[41] H. Ma. A. Kong. Y. Ji. B. He. Y. Song and J. Li. Ultrahigh adsorption capacities for anionic and cationic dyes from wastewater using only chitosan. J. Clean. Prod. (2018). https://doi.org/10.1016/j.jclepro.2018.12.217

تجزیه نوری رنگ‌های خطرناک آزو آنیونی و کاتیونی با استفاده از $AlCoFe_2O_4$ به عنوان کاتالیزور سبز

راحیل صیادی‌پور*، هما شفیعی‌خانی

دانشجوی کارشناسی ارشد، شیمی تجزیه، دانشگاه پیام‌نور، شیراز، ایران.
دکترای شیمی تجزیه، استادیار، دانشگاه پیام نور، تهران، ایران.
* E-mail: sayadipourr@gmail.com

تاریخ دریافت: ۴ مرداد ۱۴۰۴ **تاریخ پذیرش:** ۲۸ شهریور ۱۴۰۴

چکیده

فاضلاب صنایع نساجی به عنوان آلوده‌ترین نوع در میان تمامی بخش‌های صنعتی طبقه‌بندی می‌شود. در این میان، رنگ‌های آزو یکی از مهم‌ترین آلاینده‌هایی هستند که اثرات سمی متعددی، به‌ویژه خاصیت سرطان‌زایی و جهش‌زایی دارند. از این رو، توسعه یک فرایند فوتوکاتالیستی قدرتمند، سازگار با محیط زیست و کارآمد برای حذف رنگ‌های آزو ضروری است. در این مطالعه، نانوذرات فریت کبالت دوپه شده با آلومینیوم ($AlCoFe_2O_4$) به روش هم‌رسوبی به عنوان یک فوتوکاتالیست سبز برای تخریب رنگ‌های آزوی آنیونی و کاتیونی سنتز شدند. نانوذرات سنتز شده با استفاده از تکنیک‌های XRD، EDS، DRS، FESEM و VSM مشخصه‌یابی شدند. نتایج XRD نشان داد که نانوذرات دارای ساختار مکعبی با میانگین اندازه قطر کمتر از ۴۵ نانومتر هستند. میزان پایین پسماند مغناطیسی (Remanent magnetization) و نیروی وادارندگی مغناطیسی (Coercivity) در تحلیل VSM، با خواص مغناطیسی نرم نانوذرات مطابقت داشت. علاوه بر این، خواص مغناطیسی نانوذرات $AlCoFe_2O_4$ امکان جداسازی آسان فوتوکاتالیست از محیط واکنش را با استفاده از یک میدان مغناطیسی خارجی فراهم می‌کند. افزون بر این، جذب بالای $AlCoFe_2O_4$ در ناحیه نور مرئی، افزایش عملکرد فوتوکاتالیستی این کاتالیست را تحت تابش نور مرئی امکان‌پذیر می‌سازد. آزمون‌های فوتوکاتالیستی با استفاده از رنگ‌های متیل اورانژ (MO) و بیسمارک براون (BB) نشان داد که تخریب به شدت به مقدار pH (pH بهینه تقریباً ۳ برای MO و ۹ برای BB)، جذب مولکول‌های رنگ بر سطح کاتالیست و مقدار دوز کاتالیست (۰/۰۵ گرم) وابسته است. تحت شرایط بهینه‌سازی شده، تخریب MO تحت تابش UV به ۱۰۰٪ و تخریب BB به ۹۸٪ رسید. فوتوکاتالیست مذکور عملکرد بالای خود را حداقل در طی پنج چرخه حفظ کرد که نشان‌دهنده پایداری و قابلیت بازیافت آن است.

کلید واژه‌ها

تجزیه نوری، رنگ‌های آزو آنیونی و کاتیونی، فوتوکاتالیست سبز، نانوذرات مغناطیسی.

DOI: 10.30473/ijac.2026.76089.1329